International Journal of Nanoscience
Vol. 20, No. 2 (2021) 2150015 (6 pages)

DOI: 10.1142/S0219581X21500150

World Scientific
www.worldscientific.com

Synthesis, Structure and Optical Properties of NiTi Shape Memory Thin Films

Nagham M. Hamed and Saeed Naif Turki Al-Rashid*
Department of Physics, College of Education for Pure Science
University of Anbar, Iraq
**esp.saeedn.turkisntr2006@uoanbar.edu.iq*

Received 13 September 2020
Accepted 25 November 2020
Published 18 January 2021

NiTi Shape Memory Alloy (SMA) is now widely used in important applications due to its shape memory effect (SME) and biocompatibility. However, there is still a challenge to control the sizes and shapes of these nanoparticles. Here, we report on the use of pulsed laser deposition technique for the cultivation of NiTi nanoparticles on glass substrates. It discussed the implications of the case of the influence of depositing laser energy on the size of a grain of NiTi nanoparticle. The nominated effect on the optical properties of its thin-film was also discussed. X-ray diffraction (XRD) analysis revealed that the films prepared at 800 mJ, 900 mJ and 1000 mJ were amorphous structures. The Atomic Force Microscopy (AFM) results confirmed that the thin films are made up of spherical particles that are evenly distributed (in terms of size). A blueshift in the bandgap was observed in the UV–Visible absorption spectra with increase in the depositing laser energy due to the quantum confinement effect of nanoparticle formation.

Keywords: NiTi thin films; shape memory alloy; nanocrystalline; structural and optical studies.

1. Introduction

Ni-Ti alloys have been a subject of interest to many scientists and engineers in the world. Their extraordinary properties (e.g., super-elasticity and shape memory effect (SME) of the NiTi compound) have found applications in many areas of industry.[1–3] Many investigations have been done to explore the SME, annealed transformation, mechanical, electrical and tribological properties of bulk NiTi. The electrochemical behavior of the Nitinol (NiTi)-based shape memory alloys (SMAs) has also been evaluated by several research groups.[3–9] Several techniques have been used for depositing NiTi SMA thin films, such as sputtering,[10] laser ablation,[9] flash evaporation[10] and cathodic arc plasma ion plating,[11] from the practical point of view, only sputter deposition has succeeded so far and the perfect SME similar to bulk materials can be obtained.[10]

This paper aims to prepare a NiTi to SMA coating by pulsed laser deposition technique and then study the structure and optical properties of NiTi at different energy of laser deposition.

* Corresponding author.

2. Experimental Part

The samples were prepared from a target of nickel-titanium alloy using the pulsed laser deposition method. Pure materials were used from Ni and Ti with purity of 99.99% in a powder form in specific proportions (Ni 55% — Ti 45%). The proportions were measured with a sensitive scale, and then the two materials were mixed until they were homogeneous inside a mill containing balls for two hours. The mixture was pressed into tablets (Pellets) using a hydraulic press (6 tons) with a sintering temperature of 500°C, after cleaning it with alcohol to form tablets with a diameter of 2 cm and a thickness of 3 mm. Nickel-titanium alloy films have been deposited on glass slides with dimensions of (22 × 35 mm), and were used for all structural and optical measurements. The glass slides were cleaned in stages, wherein the first stage, they were washed with regular water, then washed with distilled water and then immersed in 99% high purity ethanol in an ultrasound bath for 15 min. After that, they were dried using special paper or in a thermal oven. The target of the nickel-titanium alloy was placed inside the laser coating chamber that contains a glass bell (Bell jar) with a thickness of (5 mm), a diameter of (220 mm) and a height of (450 mm) and is based on the upper base made of stainless steel square in shape with a thickness of (14 mm). The thin film deposition was carried out in a vacuum atmosphere obtained by a rotating vacuum system where the lowest pressure can be obtained from this pump, which is 10^{-3} Torr, and a vacuum controller was attached to the chamber to identify the amount of working pressure. In this process, the pulsed laser (Nd: YAG) with a pulse duration of 10 ns, and a wavelength of 1064 nm were used. The target of the NiTi alloy was irradiated with a laser beam with three different energies of 800 mJ, 900 mJ and 1000 mJ. The number of pulses used for deposition was 100 pulses and it was stable for all films and the material, to ensure different thicknesses. Thin films of NiTi were examined and the crystal structure and morphology were studied by X-ray diffraction (XRD) device (XRD-6000 Shimadzu) using Cu Kα radiations ($\lambda = 0.15406$ nm) and examining Atomic Force Microscopy (AFM) with (AA3000 scanning probe microscope, Tib NSC35/AIBS). The thin-film transmittance and absorbance spectra were also examined by the UV/Visible 2601 PC Shimadzu software 1700, 1650 Japan, spectrophotometer. It is used to find the optical constants (absorption coefficient, reflectivity, transmittance, extinction coefficient, dielectric constant with its real and imaginary parts and the optical energy gap).

3. Results and Discussion

It was found that the XRD patterns of NiTi compound alloy prepared in this work are similar to the corresponding patterns of standard compound alloy. The peaks positions (Fig. 1) and the d spacing calculated from them are in agreement with the ASTM standard (27-0344) of NiTi compound (Table 1). The analysis of peak positions and intensities showed that the Bragg reflections of NiTi alloy target correspond to the planes [110], [111], [012], [112] and [222] reflections.

It can be observed that the powder metallurgy method with sintering temperature and time is enough to complete the phase transformation and all Ni, Ti can be transformed into monoclinic NiTi phase (Martensite-NiTi) cubic NiTi phase (Austenite-NiTi). The sample then exhibits shape memory properties and hexagonal Ni_3Ti phase, which represents a harmful phase because it does not possess shape memory properties and it has more tendency to corrode than the other two phases.[12]

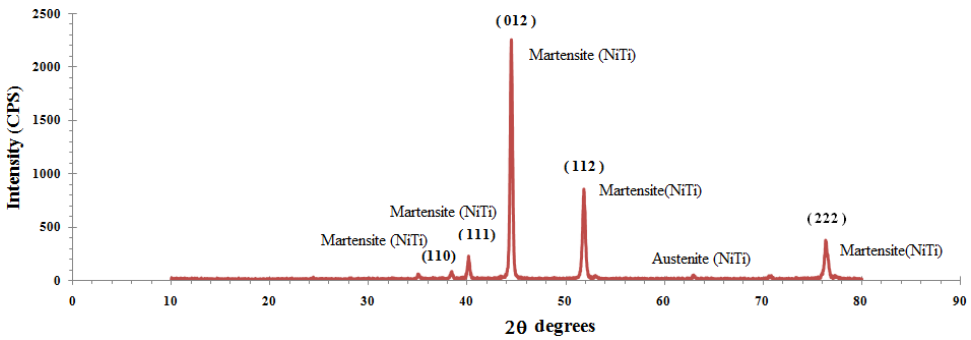

Fig. 1. XRD patterns at ambient temperature for the NiTi alloy.

Table 1. Results of the XRD measurements for the NiTi alloy.

	2θ (Deg.)	FWHM (Deg.)	d_{hkl} Exp. (Å)	Crystallite size (nm)	d_{hkl} Std.	*hkl*
NiTi	44.4725	0.2546	2.0355	33.7	2.05	(012)
	51.8198	0.2546	1.7629	34.7	1.77	(112)
	76.3491	0.2546	1.2463	39.7	1.26	(222)

XRD of the as-deposited NiTi thin films using different laser energies showed only a broad peak and no crystalline peaks appear, suggesting an amorphous structure,[13,14] as shown in Fig. 2.

Figure 3 shows the AFM images of the NiTi film samples deposited at different laser energies. It can be seen that variations are evident in the shapes and sizes of the nanograins. Moreover, it shows particles that are symmetrical and spherical with triangular, hexahedral and semi-pentagonal particles well distributed throughout the samples, sans aggregation. AFM data are shown in Table 2, where the grain sizes are (67.8–110.6 nm), while the RMS roughness is (7.39 nm and 11.4 nm). The deposited film shows broad size/shape distributions. It is also evident that the grain size and depositing laser energy are directly proportional, which could be due to increased laser energy forming smaller grains. As seen from the picture, NiTi nanoparticles are relatively evenly distributed in the copolymer matrix and this should be considered an ordinary case for the method that we use.

The Transmittance spectra of (NiTi) films in the spectral range (300–900 nm) are shown in Fig. 4(a), the percentage of transmittance increases with the increase in the pulsed laser energy. The variation is clear in the region of wavelength greater than 350 nm. This effect can be attributed to the correlation of the transmittance spectrum with the ordering of energy levels related to the crystal structure of the material as well as the general properties of the material and also the presence of defects and surface roughness that leads to the scattering of the incident radiation.[15] On the other hand, the transmittance percentage for wavelengths shorter than 340 nm is reduced by a factor of (10%) relative to the corresponding transmittance of as-deposited NiTi films. The reflectance intensity of the NiTi thin films was measured, as shown in Fig. 4(b). The reduced reflectance is achieved in the PLD NiTi film, with increase in the depositing laser energy. The reduced reflectance can be attributed to the inherent nanostructure on the surface during the PLD growth process.[16] From Fig. 4(c), we can

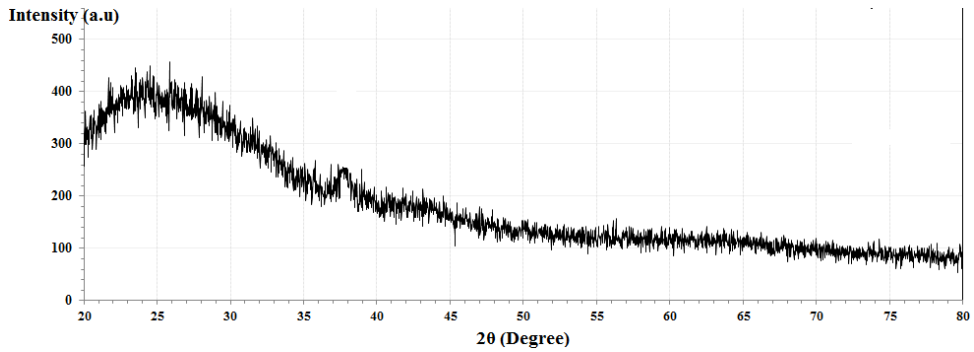

Fig. 2. Room temperature XRD profiles of deposited NiTi films using different laser energies.

Table 2. AFM surface morphologies of NiTi thin layers at different depositing laser energy.

The energies used	Roughness average (nm)	Root mean square (nm)	Average grain size (nm)
800	13.2	11.4	110.6
900	8.96	7.76	82.4
1000	8.58	7.39	67.8

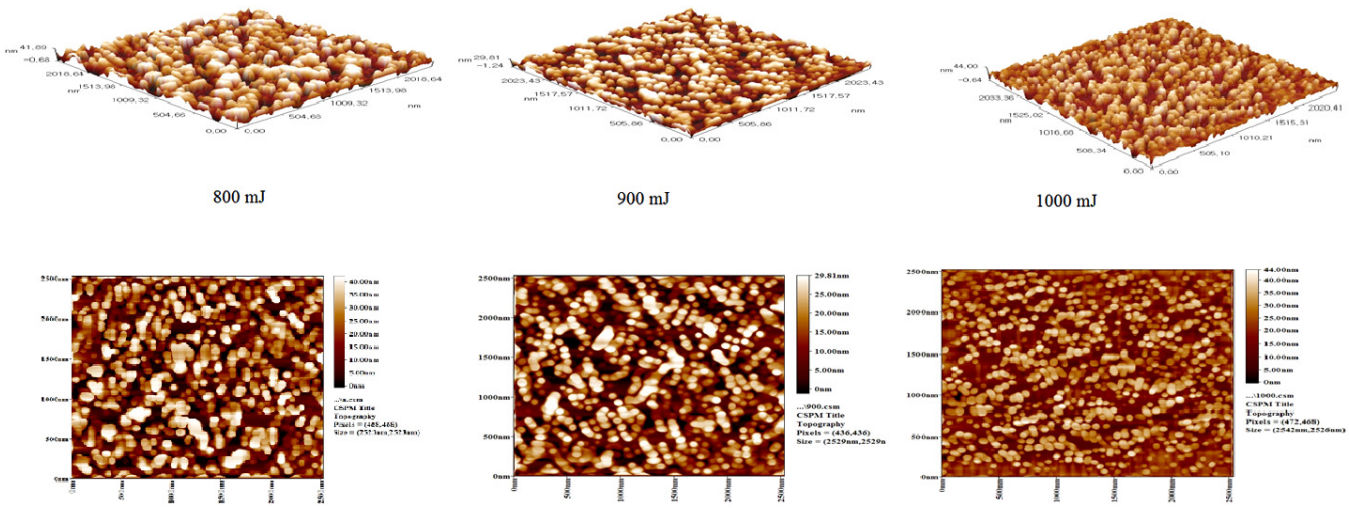

Fig. 3. AFM images of NiTi thin films deposited at different laser energy.

note the decrease in absorbance with increase in the λ for all samples. The absorbance spectral characteristics are affected by increasing laser energy, as observed with the absorbance intensity, which was decreased with the increase of laser energy. In the UV region, the absorption is more than 90%. Below the energy bandgap, the absorption is caused by the defects states. The refractive index was determined from the reflectance data. The increase of the pulsed laser energy causes an overall decrease in the refractive index as in Fig. 4(d). The decrease is due to the overall decrease in the reflectance with the increase of pulsed laser energy.[17] The absorption edge and optical energy gap have been determined from the plot of the absorption coefficient a vs wavelength. It is clear from Fig. 4(e) that there are two regions of absorption. The first region occurs at 310–370 nm and the second region starts where two exceeds 370–900 nm. The absorption coefficient takes higher values (> 10 cm) in the first region, which results from the electronic transitions of the valence band and the impurities and the transitions of energy bands. These values are reduced sharply with increase in the wavelengths. In the second region of the spectrum, the variation of absorption coefficient with wavelengths becomes slight and the values of a for all NiTi films are very close at the cut-off wavelength. The decrease in absorption coefficients with increase in the pulsed laser energy is clear. This decrease is related to a decrease in the proportion of impurities in the NiTi film. The bandgap depends on different parameters including the film structure, the arrangement and distribution of atoms in the crystal lattice. Direct energy gaps were calculated from the $(\alpha h\upsilon)^2$ and $(\alpha h\upsilon)^{1/2}$ versus photon energy, respectively, for several

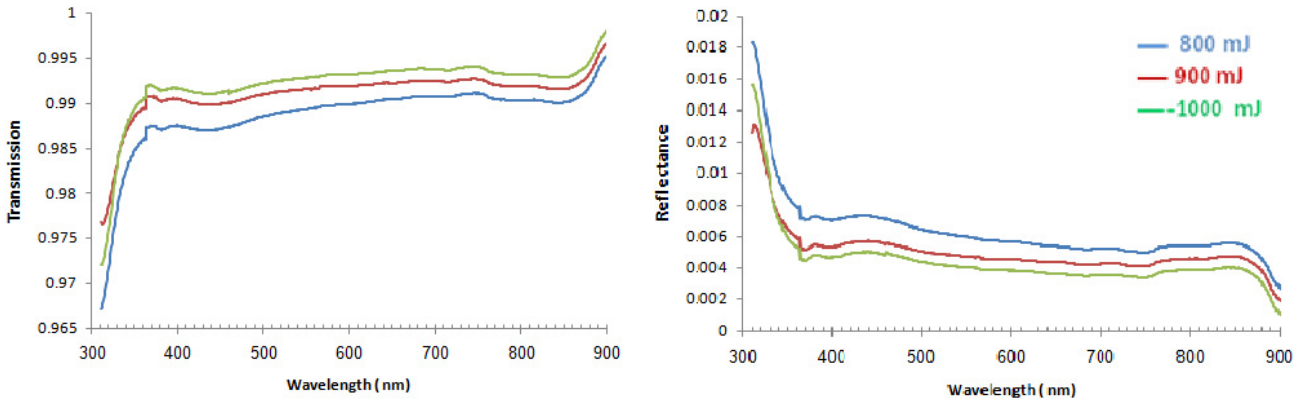

(a) (b)

Fig. 4. (a) Optical transmission, (b) absorbance, (c) reflectance spectra, (d) refractive index, (e) absorption coefficient, (f) energy gab and (g) extinction coefficient of NiTi thin films.

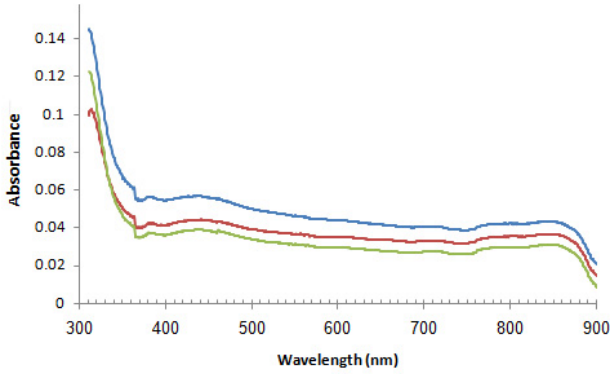

(c)

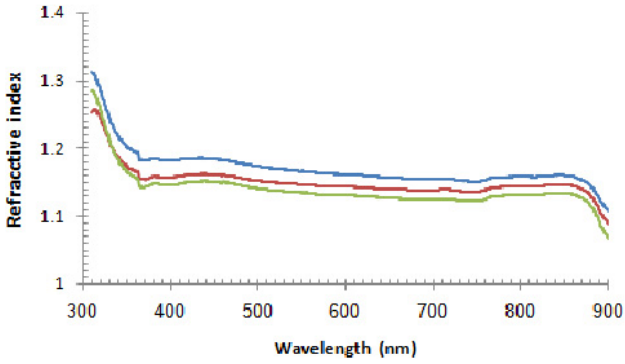

(d)

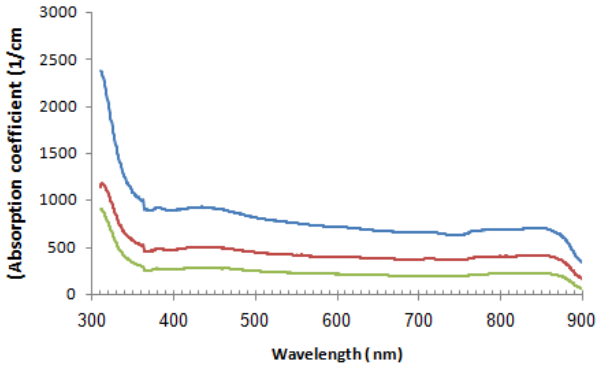

(e)

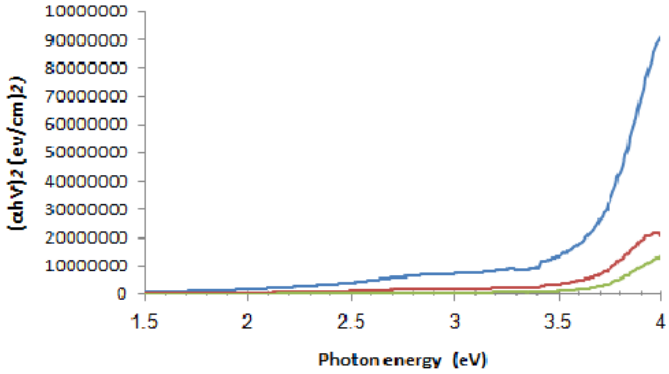

(f)

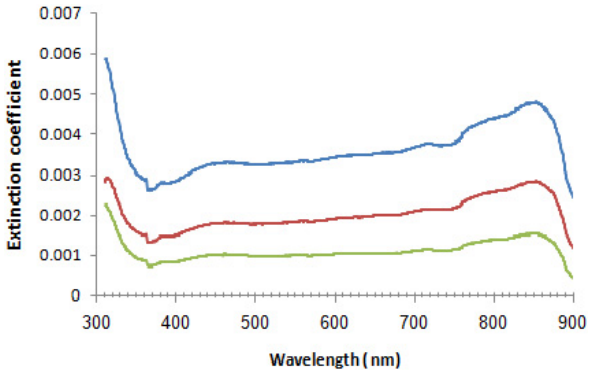

(g)

Fig. 4. (*Continued*)

deposition parameters, as illustrated in Fig. 4(f). The bandgap value was determined via extrapolating the linear region of the curves until they intercept the photon energy axis. The linear dependence of $(\alpha h\upsilon)^2$ indicated $(h\upsilon)$ is the direct energy gap. It can be observed from Fig. 4(f) that the energy gap increases with the increasing energy of laser pulse where at energy 800 mJ, the value of the energy gap is 3.67 eV and when increasing the energy to 1000 mJ, the value of the energy gap is 3.71 eV. The increase in the bandgap with annealing temperature is attributed to the increase in the packing density of thin-film and comprising very larger grains in the film. When the crystallite size increases, grain boundaries decrease minimizing the scattering and resulting in the energy bandgap increase.

This means that the low levels of the conduction band are filled with electrons. It needs high energy to excite the electrons from the valence band to the

conduction band. This causes an expansion of the optical energy gap and this could be a consequence of a size quantization effect in the sample[18,19] The extinction coefficient represents the electromagnetic wave attenuation that is propagating through the material, where its values depend on both the density of free electrons and the structural nature of the material.[20] Figure 4(g) shows the extinction coefficient as a function of wavelength for several deposition energies. The values of the extinction coefficient are directly related to the absorption of light. For all deposition energies, the figure shows a decrease in the coefficient of extinction values with an increase in the pulsed laser energy and an increase in the wavelength as a result of increased absorption,[21] where there is maximum value of the coefficient of extinction at the wavelength (300 nm). This increase indicates the occurrence of direct electronic transfers.

4. Conclusions

The study of laser energy effect on the size of produced NiTi nanoparticles confirmed that changing laser energy is a good tool to control the size of the nanoparticles where the grain size decreases with increase in laser energy from 800–1000 mJ. The optical properties show an increase in the optical bandgap with increase in laser peaks energy from 800 mJ to 1000 mJ due to quantum confinement.

References

1. L. Petrini and F. Migliavacca, *Journal of Metallurgy*, Vol. 2011 (Hindawi Publishing Corporation, 2011), Article ID 501483, 15 pages, doi:10.1155/2011/501483.
2. T. Yunxiang, Sh. Aleksandr and Z. Yufeng, *Adv. Eng. Mater.* **22**, 1900496 (2020).
3. W. Predki, A. Knopik and B. Bauer, *Mater. Sci. Eng.* **481**, 598 (2008).
4. N. El-Bagoury, M. A. Amin and H. Shokry, *Int. J. Electrochem. Sci.* **8**, 1246 (2013).
5. T. Lizhen, A. D. Richard and C. C. Wendy, *Biomaterials* **24**, 3931 (2003).
6. H. Dong, X. Ju, H. Yang, L. Qian and Z. Zhou, *J. Mater. Sci.: Mater. Med.* **19**, 937 (2008).
7. Y.-H. Li, G.-B. Rao, L.-J. Rong and Y.-Y. Li, *Mater. Lett.* **57**, 448 (2002).
8. Z. Tingting, L. Yan, X. Yan, S. V. Subbu, X. Yan and Z. Xinqing, *J. Mater. Sci.: Mater. Med.* **24**, 105 (2013).
9. A. Camilo, P. Antonio, M. Adriana, S. Enrique and J. G. Francisco, *J. Mater. Sci.: Mater. Med.* **22**, 2813 (2011).
10. S. Miyazaki and A. Ishida, *Mater. Sci. Eng. A* **273–275**, 133 (1999).
11. H. Ju-Liang, K. Won and C. Jingtang, *Thin Solid Films* **359**, 46 (2000).
12. S.-F. Ou, B.-Y. Peng, Y.-C. Chen and M.-H. Tsai, *Metals* **8**, 342 (2018).
13. G. Satoh, A. Birnbaum and Y. Lawrence, *J. Manuf. Sci. Eng.* **132**, 051004 (2010).
14. K. Ashvani, S. Devendra and K. Davinder, *Surf. Coat. Technol.* **203**, 1603 (2009).
15. J. A. Najim and J. M. Rozaiq, *Physics and Astronomy* **15**, 137, doi:10.18052/www.scipress.com/ILCPA.15.
16. C.-H. Liu, C.-H. Chen, S. Y. Chen, Y. T. Yen, W. C. Kuo, Y. K. Liao, J. Y. Juang, H. C. Kuo, C. H. Lai, L. J. Chen and Y. L. Chueh, *Nano Lett.* **11**, 4448 (2011).
17. A. M. Hassanien, A. A. Atta, M. M. El-Nahass, S. I. Ahmed, A. A. Shaltout, A. M. Al-Baradi, A. Alodhayb and A. M. Kamal, *Opt. Quantum Electron.* **52**, 194 (2020).
18. E. G. Sophie, G. Alexander, G. Dieter, B. Wolfgang, L. S. Martha and F. Christian-Herbert, *Thin Solid Films* **519**, 4298 (2011).
19. Q. M. Zamin and O. B. Narmina, *Compos.: Part B* **68**, 435 (2015).
20. S.-M. Lam, J.-C. Sin, A. Z. Abdullah and A. R. Mohamed, *Desalin. Water Treat.* **41**, 169 (2012).
21. M. P. Sarma and G. Wary, *Am. J. Mater. Sci. Technol.* **4**, 58 (2015), doi:10.7726/ajmst.2015.1005.